

Electronic Supplementary Information for

Necklace-like CNT-Co₉S₈@C-CNT for high-performance zinc-ion batteries

Yongsheng Zhou^[a], Yingchun Zhu^[b,d], and Bingshe Xu^[c]

[a] College of Chemistry and Materials Engineering, Anhui Science and Technology University, Bengbu,
233030, P. R. China

[b] Key Laboratory of Inorganic Coating Materials CAS, Shanghai Institute of Ceramics, Chinese Academy of
Sciences, Shanghai, 200050, P. R. China

[c] Key Laboratory of Interface Science and Engineering in Advanced Materials, Ministry of Education,
Taiyuan University of Technology, Taiyuan, 030024, P. R. China

[d] Center of Materials Science and Optoelectronics Engineering, University of Chinese Academy of
Sciences, Beijing 100049, P. R. China

E-mail: yszhou1981@gmail.com

Experimental section

Synthesis of CNT-Co₉S₈@C-CNT

4 mmol CoCl₂·6H₂O, 2.3 mmol CH₄N₂S, and polyacrylonitrile (PAN) (0.1 g) were dispersed in 55.5 mM glucose solution in a 40 mL glass vial with a PET cap. 3 g CoC₂O₄·2H₂O was calcined for 3.5h in air at 700 °C in a tube furnace with an air atmosphere. The obtained powder was ground and then mixed with sulfur powder with a mass ratio of 1:5, which were then placed in a graphite crucible enclosed within a graphite susceptor, and heated up to the 1000 °C using an induction furnace with a flow of Ar (1100 sccm) and H₂ (50 sccm). H₂ was allowed to bubble through the vial. The Co₉S₈@C and Co₉S₈ were synthesized by a similar procedure without using glucose and PAN.

Material Characterization

The X-ray diffractometer (XRD, Bruker D8-Advance, Cu K α , λ =0.15406 nm) was used to analyze the crystal structure of the products (CNT-Co₉S₈@C-CNT nanocomposites). Morphology and microstructure of CNT-Co₉S₈@C-CNT were revealed by field emission transmission electron microscope (FE-TEM, JEOL JEM-F200 (HR)) and field-emission scanning electron microscope (SEM, Gemini SEM 500). Thermogravimetric analysis (TGA) curves were performed on a differential scanning calorimeter (DSC, NETZSCH STA449F5) within a temperature range of 20-800 °C in air. Nitrogen adsorption-desorption test was conducted by ASAP 2020 Plus HD88 to analyze the specific surface area and pore-size distribution of Co₉S₈, Co₉S₈@C and CNT-Co₉S₈@C-CNT.

Electrochemical measurements

The CNT-Co₉S₈@C-CNT cathodes and other control materials were mixed with Super P and polyvinylidene fluoride (PVDF) at a weight ratio of 7:2:1 in N-methyl pyrrolidone (NMP). Then, the slurry was pressed into a suitable film and dried under vacuum at 60 °C, and subsequently pressed a quantified thin membrane onto a titanium meshes (d = 14 mm). The active materials mass-loading was about 2 mg cm⁻², and the CNT-Co₉S₈@C-CNT cathodes with high mass-loading (about 5 and 10 mg cm⁻²) were also prepared. The AZIBs was assembled using prepared CNT-Co₉S₈@C-CNT cathode, glass fiber membrane and Zn foil anode (0.05 mm) with 3 m Zn(CF₃SO₃)₂ aqueous electrolytes (m: mol kg⁻¹).

Cyclic voltammetry (CV), and electrochemical impedance spectroscopy (EIS) were investigated on a Bio-Logic VSP-300 electrochemical workstation (France). The galvanostatic discharge/charge process were operated on a Land battery test system (LAND BT2001) in 0.2-1.6 V voltage range. Additionally, the long cycle performance and rate capability at different current density were collected using Hukuto Denko battery system (HJ series, Japan). The low temperature electrochemical performance was tested in the Meiling Biology & Medical DW-HW50 ultralow freezer, while the oven was employed on high temperature testing.

Computational methods

All calculations in this work were performed using Gaussian 09 program package. Full geometry optimizations were performed to locate all the stationary points, using the B3LYP with the def2svp basis, namely B3LYP/def2svp. Dispersion corrections were computed with Grimme's D3(BJ) method in optimization. Harmonic vibrational frequency was performed at the same level to guarantee that there is no imaginary frequency in the molecules, i.e. they locate on the minima of potential energy surface. Convergence parameters of the default threshold were retained

(maximum force within 4.5×10^{-4} Hartrees/Bohr and root mean square (RMS) force within 3.0×10^{-4} Hartrees/Radian) to obtain the optimized structure. The optimal structure was identified given that all calculations for structural optimization were successfully converged within the convergence threshold of no imaginary frequency, during the process of vibration analysis.

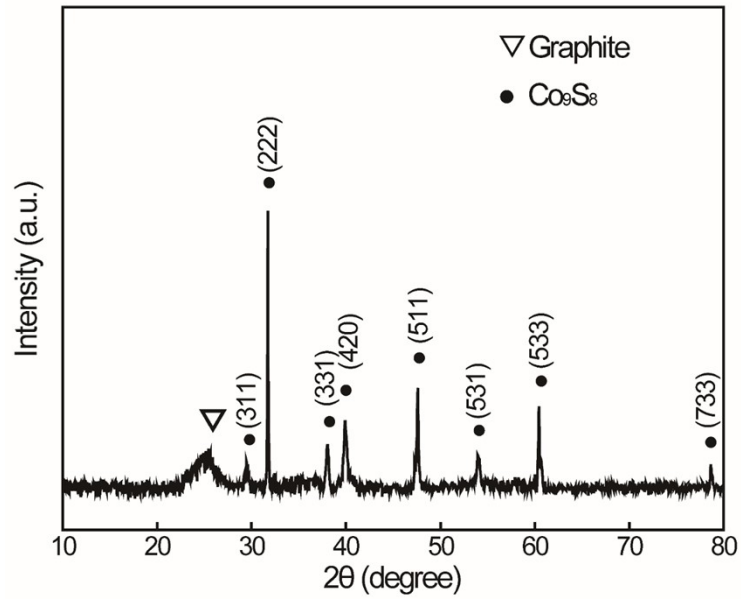


Figure S1. XRD pattern of the CNT-Co₉S₈@C-CNT.

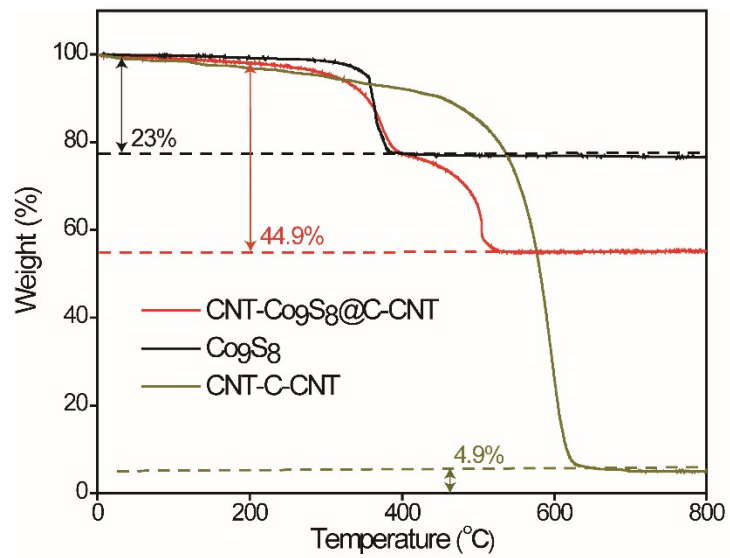


Figure S2. TGA curves of CNT-Co₉S₈@C-CNT, Co₉S₈, and CNT-C-CNT.

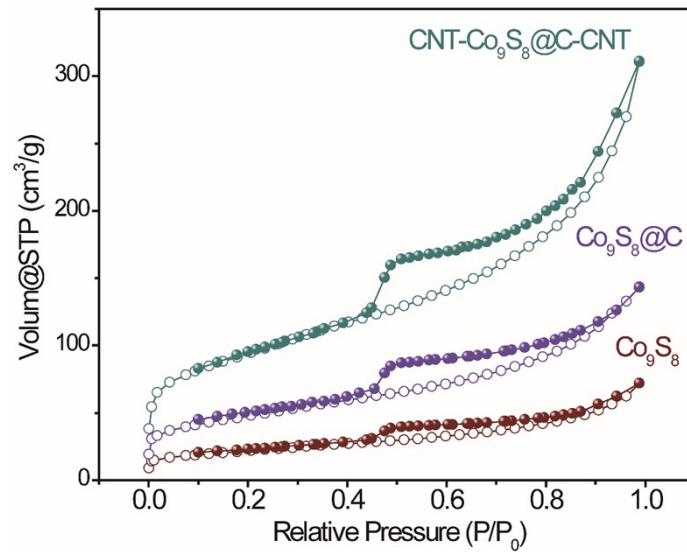


Figure S3. The Nitrogen adsorption-desorption isotherms of the CNT-Co₉S₈@C-CNT, Co₉S₈@C, and Co₉S₈ at 77.3 K.

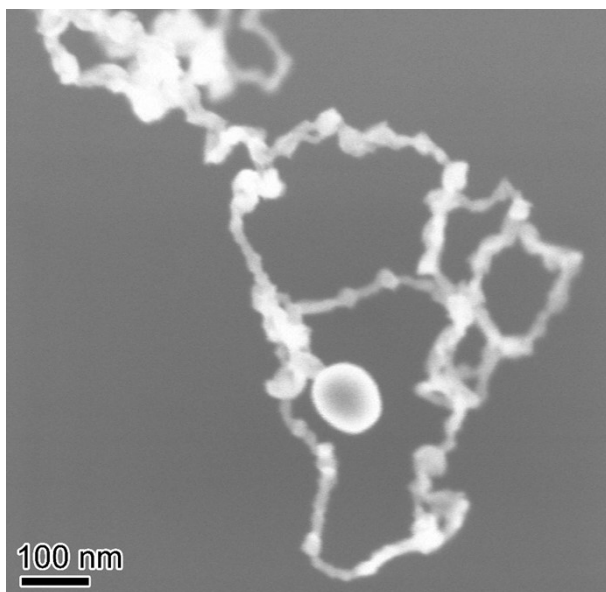


Figure S4. SEM image of CNT-Co₉S₈@C-CNT after 1000 cycles at 5 A g⁻¹.

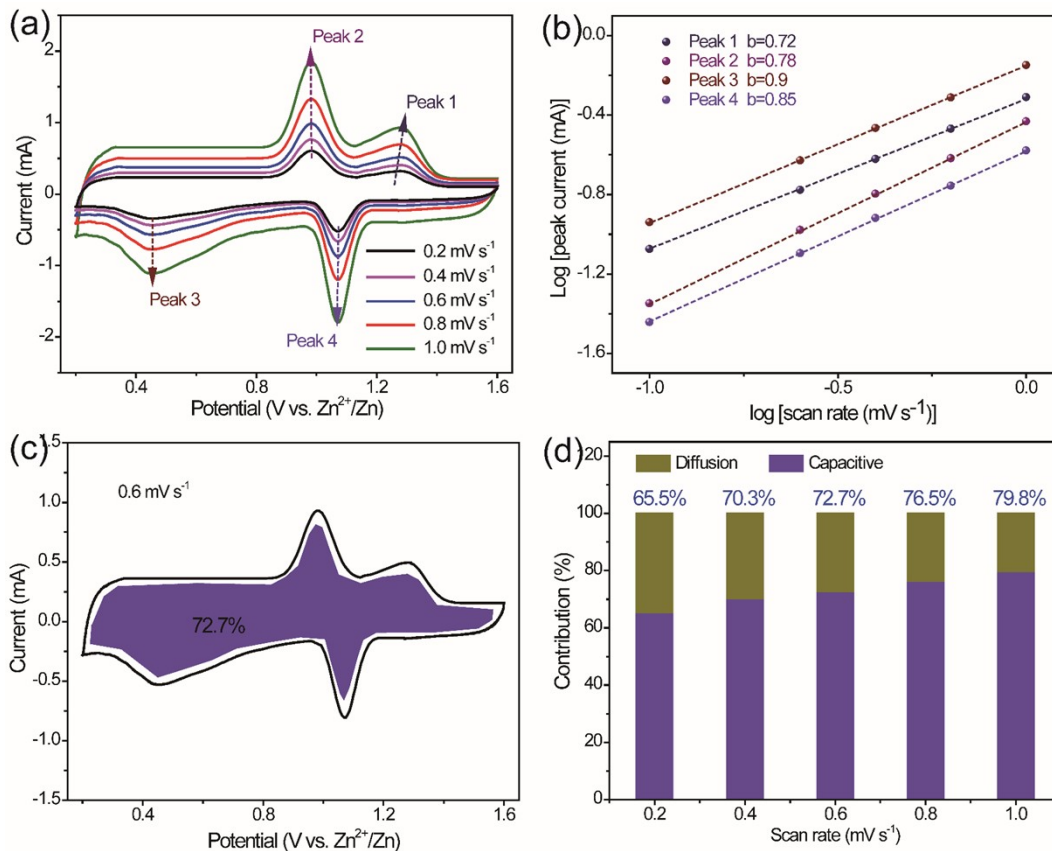


Figure S5. (a) CV profiles at different scan rates, (b) log (peak current) versus log (scan rate) at various scan rates, (c) capacitive contribution (green area) at 1 mV s^{-1} , and (d) the contribution ratio of capacitive capacity at different scan rates for $\text{Co}_9\text{S}_8@\text{C}$.

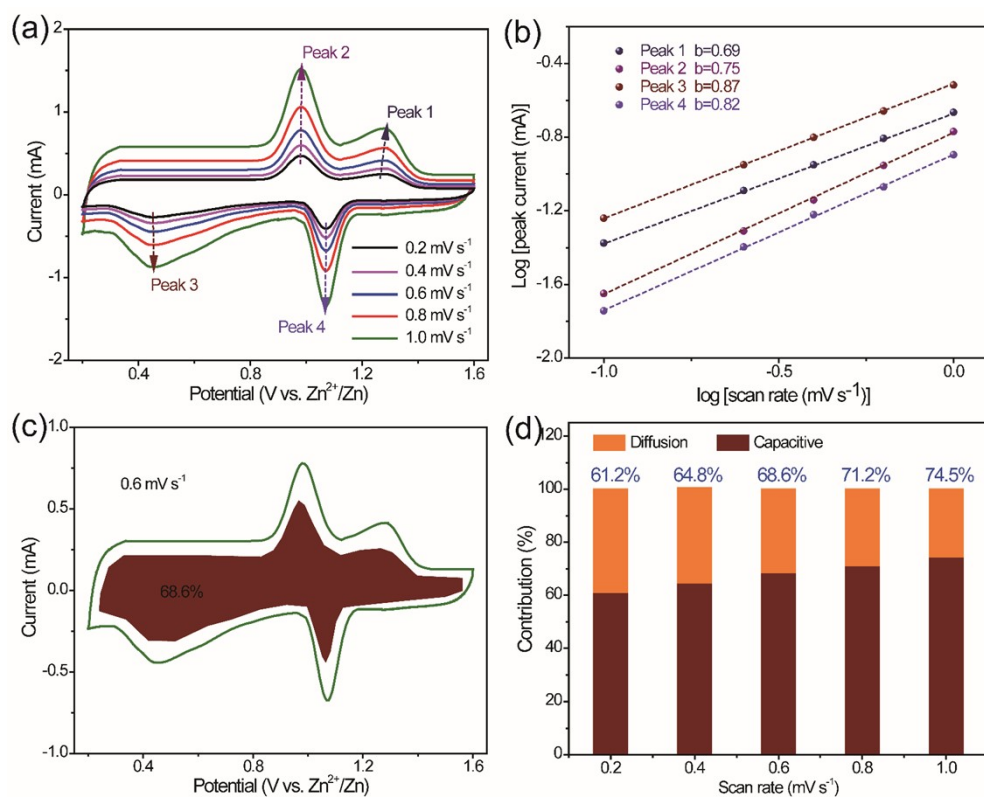


Figure S6. (a) CV profiles at different scan rates, (b) log (peak current) versus log (scan rate) at various scan rates, (c) capacitive contribution (pink area) at 1 mV s^{-1} , and (d) the contribution ratio of capacitive capacity at different scan rates for Co_9S_8 .

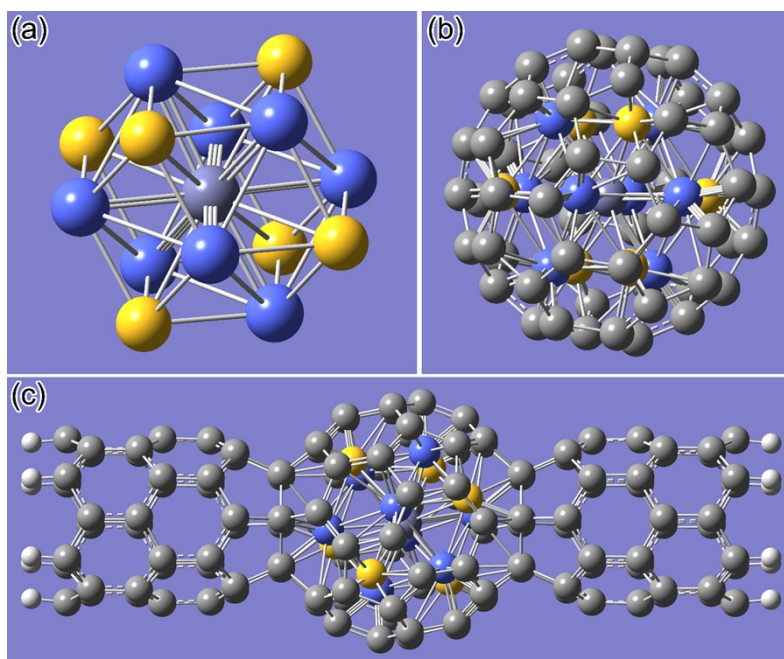


Figure S7. Basic model of Zn^{2+} inserted in (a) Co_9S_8 , (b) $Co_9S_8@C$, and (c) CNT- $Co_9S_8@C$ -CNT.

Materials	Stable Capacity	Rate	Cycling	References
MWCNTs@a-C@MoS ₂	176 mA h g ⁻¹ at 0.5 A g ⁻¹	181 mAh g ⁻¹ at 0.1 A g ⁻¹	95 mAh g ⁻¹ at 5 A g ⁻¹ for 1000 cycles	1
CC@NC-NiCo ₂ S ₄	0.58 mAh cm ⁻² at 2 mA cm ⁻²	228 mAh g ⁻¹ at 0.8 A g ⁻¹	175 mAh g ⁻¹ at 4.65 A g ⁻¹ for 1000 cycles	2
V ₃ S ₄ @C	340 mAh g ⁻¹ at 0.2 A g ⁻¹	N/A	150 mAh g ⁻¹ at 5 A g ⁻¹ for 1000 cycles	3
VS ₂ /Ti ₃ C ₂ Tz	285 mAh g ⁻¹ at 0.2 A g ⁻¹	N/A	N/A	4
ZnV ₂ S ₄	348.2 mAh g ⁻¹ at 0.5 A g ⁻¹	307.6 mAh g ⁻¹ at 1 A g ⁻¹	235.8 mAh g ⁻¹ at 4 A g ⁻¹ for 1000 cycles	5
VS ₄ /VOx@C	350 mA h g ⁻¹ at 0.1 A g ⁻¹	156 mA h g ⁻¹ at 10 A g ⁻¹	145 mAh g ⁻¹ at 10 A g ⁻¹ for 1000 cycles	6
MoSSe/rGO	272.6 mA h g ⁻¹ at 0.1 A g ⁻¹	253.8 mA h g ⁻¹ at 0.2 A g ⁻¹	115.1 mAh g ⁻¹ at 2 A g ⁻¹ for 1200 cycles	7
Co-Ni ₃ S _{2-x}	183.9 mAh g ⁻¹ at 1 A g ⁻¹	N/A	N/A	8
Our work	250.8 mA h g ⁻¹ at 0.5 A g ⁻¹	426.2 mAh g ⁻¹ at 0.1 A g ⁻¹	302.7 mAh g ⁻¹ at 5 A g ⁻¹ for 5000 cycles	

Table S1 Comparison of metal sulfide-based cathodes materials for AZIBs with literature.

References

1. F. E. Niu, Z. C. Bai, Y. Y. Mao, S. Q. Zhang, H. R. Yan, X. Xu, J. M. Chen, N. N. Wang. *Chem. Eng. J.* 2023, **453**, 139933.
2. Z. X. Cui, J. X. Zhou, X. L. Wang, Q. T. Wang, J. H. Si, X. L. Liu. *Adv. Compos. and Hybrid Mater.* 2023, **6**: 95.
3. N. N. Yu, B. Sun, M. Li, L. Xu, W. Y. Wang, F. X. Wei, Y. W. Sui, L. F. Cheng, S. Q. Wang. *J. Energy Storage* 2024, **94**, 112284.

4. L. P. Zhang, Y. Y. Li, X. J. Liu, R. P. Yang, J. X. Qiu, J. K. Xu, B. Y. Lu, J. Rosen, L. Q. Qin, J. X. Jiang. *Adv. Sci.* 2024, **11**(25), 2401252.
5. M. Narayanasamy, B. Balan, C. Yan, S. Angaiah. *Chin. Chem. Lett.* 2023, **34**(8), 108076.
6. J. Xu, H. B. Guo. *CrystEngComm* 2023, **25**(6), 998-1005.
7. H. Li, B. Chen, R. H. Gao, F. G. Xu, X. Z. Wen, X. W. Zhong, C. Li, Z. H. Piao, N. T. Hu, X. Xiao, F. Shao, G. M. Zhou, J. L. Yang. *Nano Res.* 2023, **16**(4), 4933-4940.
8. X. J. Li, S. S. Zhao, G. M. Qu, X. Wang, P. Y. Hou, G. Zhao, X. J. Xu. *J. Mater. Sci. Technol.* 2022, **118**, 190-198.